Microfluid Nanofluid (2013) 14:499–508
DOI 10.1007/s10404-012-1068-6

RESEARCH PAPER

A novel method to construct 3D electrodes at the sidewall of microfluidic channel

Shunbo Li · Ming Li · Yu Sanna Hui · Wenbin Cao · Weihua Li · Weijia Wen

Received: 24 July 2012 / Accepted: 20 September 2012 / Published online: 7 October 2012

Abstract We report a simple, low-cost and novel method for constructing three-dimensional (3D) microelectrodes in microfluidic system by utilizing low melting point metal alloy. Three-dimensional electrodes have unique properties in application of cell lysis, electro-osmosis, electroporation and dielectrophoresis. The fabrication process involves conventional photolithography and sputtering techniques to fabricate planar electrodes, positioning bismuth (Bi) alloy microspheres at the sidewall of PDMS channel, plasma bonding and low temperature annealing to improve electrical connection between metal microspheres and planar electrodes. Compared to other fabrication methods for 3D electrodes, the presented one does not require rigorous experimental conditions, cumbersome processes and expensive equipments. Numerical analysis on electric field distribution with different electrode configurations was presented to verify the unique field distribution of arc-shaped electrodes. The application of 3D electrode configuration with high-conductive alloy microspheres was confirmed by particle manipulation based on dielectrophoresis. The proposed technique offers alternatives to construct 3D electrodes from 2D electrodes. More importantly, the simplicity of the fabrication process provides easy ways to fabricate electrodes fast with arc-shaped geometry at the sidewall of microchannel.

Keywords Microfluidics · Three-dimensional electrodes · Low melting temperature Bi alloy · Dielectrophoresis (DEP) · Particle manipulation

S. Li · W. Wen (✉)
Department of Physics, The Hong Kong University of Science and Technology, Clear Water Bay, Kowloon, Hong Kong
e-mail: phwen@ust.hk

M. Li · W. Li (✉)
School of Mechanical, Materials and Mechatronic Engineering, University of Wollongong, Wollongong, NSW 2522, Australia
e-mail: weihuali@uow.edu.au

Y. S. Hui · W. Cao · W. Wen
Nano Science and Technology Program and Department of Physics, The Hong Kong University of Science and Technology, Clear Water Bay, Kowloon, Hong Kong

1 Introduction

Microfluidics has attracted much attention for years due to its low fabrication cost, good analytical performance, low material consumption, high sensitivity and fast detection (Whitesides 2006). As a crucial component in lab-on-a-chip device, embedded electrodes play an essential role in several processes such as electrochemical reaction, electric detection, cell lysis, electroporation, electro-osmosis, electrophoresis and dielectrophoresis (Yu et al. 2007; Gong et al. 2010; Zeng et al. 2011; Mahalanabis et al. 2009; Wu et al. 2008; Pethig 2010; Li et al. 2012). Thus, the geometry and layout of electrodes have become pronounced in microfluidic systems. Originating from the MEMS technique, most of the microfabrication processes are planar-based patterning, which are fabricated by conventional photolithography, followed by metal deposition and lift-off processes. Metal deposition by sputtering or evaporation has its limits, such as film thickness and electrode profile along the vertical direction cannot be designed and controlled in the range of micrometers comparable to microfluidic channels. 3D electrodes, however, show unique and excellent advantages in microfluidic devices. Lu et al. (2006) showed that the geometry of 3D electrode demonstrated significantly higher lysis efficiency than 2D electrodes from simulation and experimental results in the

study of cell lysis via electroporation. Numthuam et al. (2011) showed that 3D micropillar electrodes significantly improved the detection current in ELISA experiments. Huang et al. (2010) developed an integrated AC electro-osmotic microfluidic pump with an optimized 3D stepped electrode array. Senousy and Harnett (2010) improved the flow rate and frequency range of AC electro-osmotic pumps by adopting 3D electrodes and comparing the results from 2D stepped electrodes made by a non-photolithographic electrode patterning method. 3D electrodes also demonstrated their advantages in particle manipulation by dielectrophoresis (DEP). Several groups (Park et al. 2005; Wang et al. 2007; Cheng et al. 2007; Iliescu et al. 2009; Cetin et al. 2009; Lewpiriyawong et al. 2010; Ma et al. 2011; Lewpiriyawong and Yang 2012) have studied the influence of different topography of 3D electrodes on cell focusing, trapping, sorting, detecting and microfluidic flow cytometry in microfluidic devices. Considering the application of different electrode configurations in the area of dielectrophoresis (DEP) as an example, microelectrodes that are deposited at the bottom of the microchannel create non-uniform electrical fields along the vertical/height direction. Such electrode configuration results in vertical DEP forces acting on the particles. The DEP forces can either attract the particles toward the bottom electrodes or repel them in the opposite direction depending on whether the DEP force is positive or negative. Since the electric field decays exponentially with the distance away from the electrodes, particles that are far away from the electrodes will exhibit less DEP force which is not sufficient to manipulate particles. The above limitations can be overcome by design and fabrication of 3D electrodes.

The ability to fabricate 3D electrodes extends the realm of electrical manipulation in microfluidics and provides many advantages that cannot be achieved by simple planar electrodes. Different fabrication methods of 3D electrodes in microfluidic chips have been developed and demonstrated. Voldman et al. (2002) developed electroplated 3D metal pillars to improve the trapping performance by DEP. Iliescu et al. (2005) demonstrated highly doped 3D silicon electrodes for DEP manipulation. However, it is not easy to obtain electrical connection via non-planar surface passing through microfluidic channel by this method. Park and Madou (2005) had developed 3D carbon SU-8 electrodes for DEP extraction of nanofibrous carbon from oil. This method must be conducted at high temperature (>900 °C) and N_2 environment protection. Fabrication of electrodes on the walls of an elliptical microfluidic channel was demonstrated by using multi-step optical lithography including wet etching on glass and metal deposition (Yu et al. 2005). It has the disadvantages of being a cumbersome process and having long fabrication time. Choi et al. (2010) proposed an ion-implantation process to pattern 3D electrodes in PDMS for particle alignment. However, this technique requires high vacuum and high voltage and also it has the risk of changing the property of PDMS after ion-implantation. Niu et al. (2007) proposed a new method to pattern PDMS-based conducting composites by mixing high concentration of silver or carbon with PDMS. But the conductivity is relatively not easy to control and the aspect ratio is lower than other methods. Herein, we proposed a novel method to construct 3D arc-shaped microelectrodes at the sidewall of microfluidic channel by utilizing a low melting point bismuth (Bi) metal alloy. The functionality of 3D electrodes fabricated by this method was demonstrated by particle manipulation and separation. This method offers many advantages such as good conductivity, low cost, simple fabrication and time saving, since the process resembles the fabrication method used for planar electrodes, favorable in DEP application due to the large electric field gradient produced by arc-shaped 3D electrodes and improvement of topological electrode design.

2 Experiments

2.1 Fabrication method

Figure 1 shows the fabrication process of a microfluidic chip with 3D arc-shaped electrodes embedded at the sidewall of the microchannel. The major fabrication steps include: (a) SU-8 mold fabrication, (b) planar electrodes patterning, (c) fabrication of microchannels with microspheres positioning at the sidewall, (d) plasma bonding and (e) thermal post-treatment.

2.1.1 SU-8 mold fabrication

The first step involved conventional photolithography: a negative photoresist SU-8 2050 was spin coated at a speed of 1,300 rpm for 30 s on a cleaned silicon (Si) wafer, giving a thickness of 100-μm SU-8 film, which was followed by pre-bake at 65 °C for 15 min and 95 °C for 20 min, UV exposure 40 s using ABM #2(ABM, San Jose, CA), post-bake at 65 °C for 5 min and 95 °C for 10 min and photoresist developing.

2.1.2 Planar electrodes patterning

Standard photolithography, sputtering and lift-off process were performed to pattern the planar electrodes on the glass substrate. The glass substrate was pre-cleaned with RCA-1 solution (mixture of deionized (DI) water, ammonium hydroxide (NH_4OH) and hydrogen peroxide (H_2O_2) in a 5:1:1 ratio), followed by rinsing three times in DI water. Then, the glass substrate was processed in sequence by spin

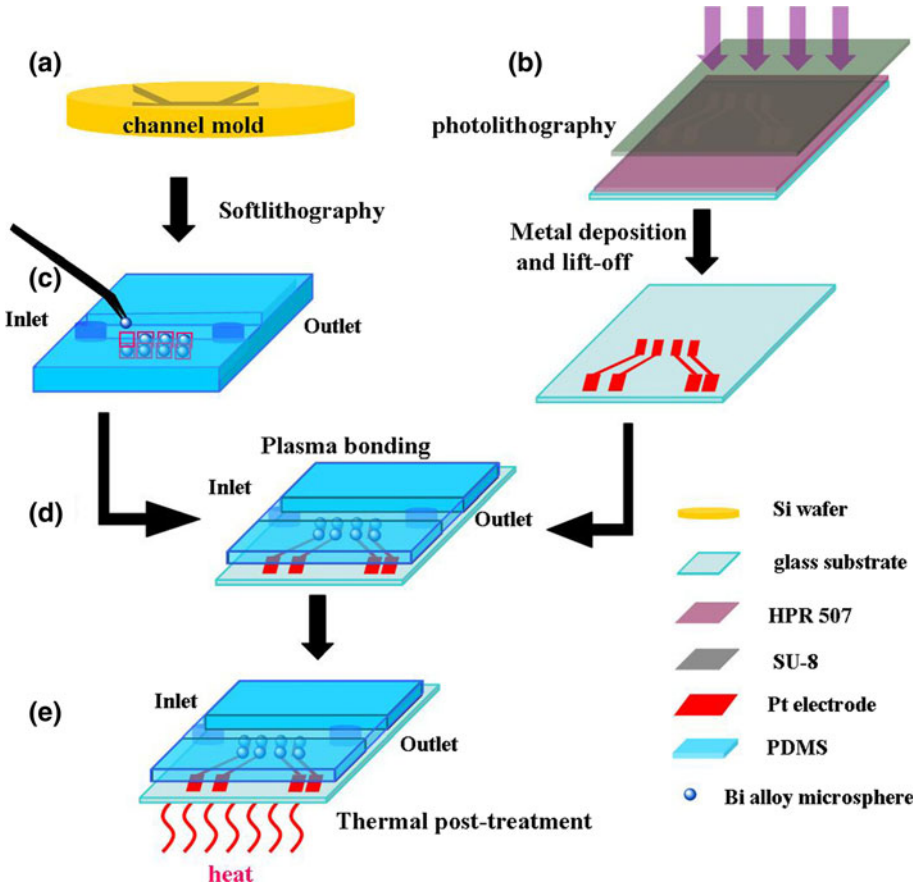

Fig. 1 Schematic of the fabrication process including: **a** SU-8 mold fabrication, **b** planar electrode patterning, **c** fabrication of microchannel with metal alloy microsphere position (PDMS recesses are highlighted by *red squares*), **d** plasma bonding, and **e** thermal post-treatment

coating positive photoresist HPR 507 at a spin speed of 2,000 rpm, soft baking on hotplate at 110 °C for 2 min, UV exposure by Mask Aligner (ABM #2) for 20 s, photoresist developing using FHD-5 for 60 s, and post-baking on hotplate at 110 °C for 2 min. The planar electrodes made of 15 nm Ti/150 nm Pt were then sputtered and patterned using the lift-off process.

2.1.3 *Fabrication of microchannels with microspheres positioning at the sidewall*

Bismuth (Bi)-based 117 alloy purchased from Rotometals (USA) is composed of Bi 40.63 %, Pb 22.1 %, In 18.1 %, Sn 10.65 % and Cd 8.2 %. The melting point of the alloy is documented at 46.5 °C (data provided by the company—Rotometals). The conductivity of this kind of metal alloy is found to be 2.23×10^6 S/m, which is comparable to most kinds of metals (data provided by Rotometals). Bi alloy microspheres were formed by a droplet generator, which is composed of a small robotic arm and a glass capillary connected to a Venturi tube. It is similar to the commercial product—Nano-Plotter (GeSiM). A small drop of molten Bi alloy was first picked up by the robotic arm and then placed into a cooling bath. The droplet will automatically form a sphere shape due to surface tension. The size of the Bi alloy microsphere is controlled by the amount of molten alloy. This method could be used to achieve mass production of metal spheres. It is capable of producing more than 1,000 spheres in an hour.

Microchannels with deep recesses (highlighted by red squares in Fig. 1), at the sidewall where the 3D electrodes were located, were made of polydimethylsiloxane (PDMS) with soft lithography (Xia and Whitesides 1998). PDMS (Dow Corning Corporation, Miland, USA) mixture with a 10:1 weight ratio of base:curing agent was first applied to the fabricated SU-8 mold. After curing in an oven at 60 °C for about 2 h, the PDMS slab was peeled off and metal microspheres with a diameter of 110 μm, which is 10 μm larger than the size of recesses, were manually positioned in the deep recesses of the PDMS layer using an optical microscope (Olympus SZX16). The purpose of this design is to increase the adhesion force between Pt electrodes and alloy spheres and then obtain a good electric connection. The position process consists of three steps: (1) metal alloy spheres are picked up by a tweezer with a sharp tip; (2) they are transferred to PDMS recesses in which spheres will automatically drop when they are moved around; (3) excess spheres that are not positioned in PDMS recesses are wiped off. All processes were conducted under an optical microscope. PDMS recesses were used to precisely position spheres.

2.1.4 Plasma bonding

The bonding step was performed between the PDMS layer containing microchannels with metal microspheres and the bottom substrate patterned with planar electrodes. The PDMS slab with fluidic inlets and outlets and Pt electrodes patterned glass substrate were treated in a plasma cleaner (Harrick Plasma PDC-002) for 1 min, after which the surface was sprayed with methanol which acted as a lubricant for latter alignment using an optical microscope. In order to evaporate methanol and improve the bonding strength between PDMS and glass substrate after aligning, the microfluidic chip was heated on a hotplate located near the microscope at 45 °C for 5 min, in which the annealing temperature was not high enough to melt the metal microspheres. It is noted that methanol will evaporate very fast (in <30 s) at room temperature. Thus, the position was almost fixed when the chip was moved to the hotplate. This heating process was used to assist in the complete evaporation of methanol and increase the adhesion force between PDMS and glass substrate after plasma.

2.1.5 Thermal post-treatment

To improve the electrical contact between the metal microspheres and planar Pt electrodes, the chip was cured in an oven at 60 °C for 10 min. Bi microspheres will bond to Pt electrodes after this thermal treatment. The accuracy of the curing temperature is critical in this process, because the solid microspheres might melt and collapse if the temperature is too high, whilst there will be no improvement in the electrical contact if the temperature is too low. Figure 2 compares the effect of annealing temperature on the shape of the 3D electrodes. The microfluidic chip in Fig. 2a was cured in an oven at 75 °C for 10 min. It is clearly seen that the spheres on the sidewall have melted and collapsed which might destroy the main channel. Figure 2b shows the microfluidic chip after annealing at 60 °C for 10 min. Compared with Fig. 2a, the shape of the alloy spheres was maintained and it had good electric contact with the planar electrodes underneath, which was proved by the following experiments.

2.2 Sample preparation and experiment setup

Cells of *Saccharomyces cerevisiae* (yeast cells) and two types of polystyrene (PS) particles were used in this study: 10-μm fluorescent polystyrene particles (Invitrogen, CA, USA) and 5-μm polystyrene particles (Sigma-Aldrich). The 5-μm particles were similar in size to the yeast cells. The cells and particles were suspended in pH 7.0 buffer solution composed of disodium hydrogen phosphate and potassium dihydrogen phosphate (Radiometer Copenhagen, Denmark)

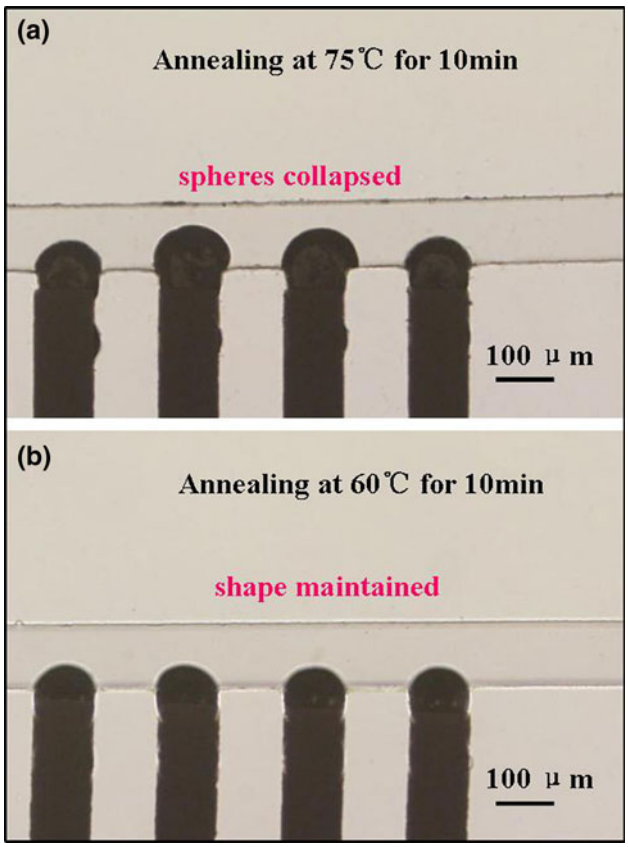

Fig. 2 Comparison of the arc-shaped electrodes at the sidewall of microchannel after annealing at 75 °C for 10 min (**a**) and annealing at 60 °C for 10 min (**b**)

before the DEP experiments. The conductivity of the suspending media was adjusted to be 380 μS/cm. Yeast cells were cultured on agar plate directly. To prepare the yeast suspensions, yeast colonies on yeast extract (YE) agar plate were scratched down and transferred to pH 7.0 buffer solutions.

For particle separation experiments, two sample solutions were prepared: (1) separation of 10 and 5-μm polystyrene particles in a 380 μS/cm buffer solution based on the size effect on DEP; (2) live yeast cells and 5-μm polystyrene particles in a 380 μS/cm buffer solution. Each sample solution was injected into the microchannel by a syringe pump (KDScientific, 781200) to maintain continuous flow. There are two inlets in our device. Thus, two syringe pumps were used to inject sample solutions. A function generator (HP 33120A) and an AC amplifier (Stereo Power Amplifier 216THX) were used as power supply. The waveform of the input signal was monitored by an oscilloscope (Tektronix TDS 2012B). Soldering technique was used to connect the power supply to the device. The motions of the cells and polystyrene particles were monitored using an inverted optical microscope (Olympus IX71, Tokyo, Japan) and recorded by a CCD camera

(Olympus DP70, Tokyo, Japan). Scanning electron microscope pictures were taken by JSM-6390 (JEOL).

3 Results and discussions

3.1 Comparison of electric field distribution for different electrode configurations

To characterize the electric field effect-related phenomenon of different electrode configurations, finite element numerical simulation (COMSOL 4.2) was performed to study the topology effect of electrode on electric field distribution. A simplified 2D geometry was used for comparing the electric field distribution for line, rectangular protrusion and arc-shaped electrodes. Here, we briefly introduce the how to perform simulation by COMSOL 4.2. First, 2D model electrostatics (es) in AC/DC section and stationary studies were selected. Then, the geometry of the channel and electrodes was defined in graphics section, followed by selecting appropriate materials for each domain and setting electric potential on the boundary of each electrode. Computing was then performed with default setting of the mesh. After that, the results were obtained by both surface and contour of square of the electric field, as determined by the expression—es.Ex^2 + es.Ey^2.

As illustrated in Fig. 3a–c, non-uniform electrical field can be generated across the width of the channel (lateral direction) when the electrodes are located at the sidewall. The generated DEP force can be used to deflect cells and particles in the lateral direction. Since many microfluidic devices are based on planar electrodes which only have large DEP force near the electrodes in the vertical direction, lateral electrodes generating large DEP force in the whole region along the height direction are more desirable for on-chip analysis, particle manipulation and parallel processing of samples.

The topology of electrodes is crucial for applications based on non-uniform electric field such as DEP. Figure 3a–c compares the results of the numerical simulation of three types of electrode configurations [(a) line electrodes, (b) rectangular protrusion and (c) arc-shaped electrodes aligning on the edge of the microchannel]. For better representation of the field distributions, the region containing two middle electrodes were illustrated in this figure. It is noted that DEP force is proportional to the divergence of the square of the electric field and it is represented by the density of contours in Fig. 3 (higher density indicates larger DEP force). The channel width is 100 μm, the protrusion of electric potential lines from the sidewall toward the center of the channel is 30 μm and the distance between two electrodes' center lines is 200 μm. Figure 3b, c indicates that the rectangular protrusion and arc-shaped electrodes result in a higher electric field and thus a large gradient of electric field in the lateral direction than that of the line electrode configurations shown in Fig. 3a, owing to the protrusion of electrodes into the channel region. Compared to rectangular protrusion (Fig. 3b), arc-shaped electrode (Fig. 3c) has a smoother electric field in region 1 and region 2 as illustrated in Fig. 3b, c. The arc-shaped electrodes therefore provide a better non-uniform electric field distribution due to the larger effective area where the DEP force was acting. Our simulation results were

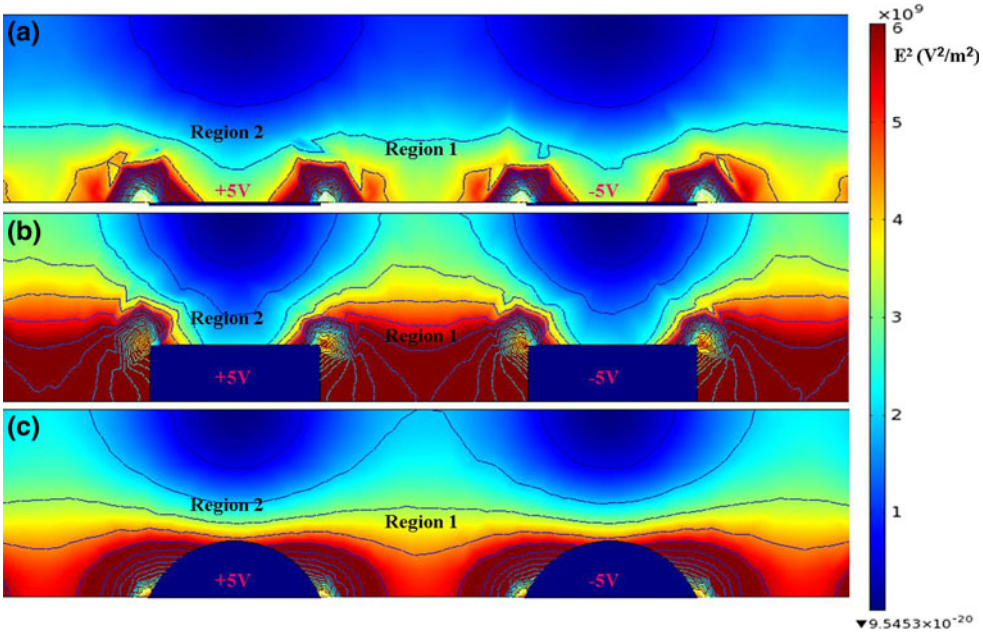

Fig. 3 Comparison of square of electric field (E^2) with different electrode configurations at the sidewall of microchannel: **a** line electrodes, **b** rectangular protrusions and **c** arc-shape electrodes. The largest protrusion is 30 μm from the edge of the channel. The width of channel is 100 μm. Both of them in **c** are the same as the real picture in our experiment. The applied voltages are +5 and −5 V, respectively, on these two electrodes

consistent with the results demonstrated by Chunag et al. (2009). The major drawbacks of rectangular protrusion configuration are the difficulties in fabrication processes and electric field divergence induced by sharp corners, which may affect cell viability. Therefore, an arc-shaped electrode is more favorable for DEP applications, since it produces a large DEP force in both regions 1 and 2 (specified in Fig. 3).

3.2 Microfluidic chip fabricated by the described method

Based on the above simulation results, a new microfluidic chip with 3D arc-shaped electrodes was fabricated. The ability to fabricate 3D electrodes provides many advantages that cannot be achieved by simple planar electrodes, especially in manipulating particles by an electric field. We have developed a process to pattern electrodes at the sidewall of the microchannel, so that the electrodes are integrated as a part of the channel sidewalls and will not interfere with the flow within the channel. In the proposed method, a single layer of photoresist (SU-8) photolithography, metal deposition and positioning of bismuth alloy microspheres were used to make the microchannel and 3D electrodes, respectively. Joule-heating effect in our device was also reduced, because the gradient of electric field is large and the driving voltage is relatively small compared to other types of electrodes in the application of particle manipulation.

Figure 4a shows the fabricated microfluidic chip that consists of a 100-μm wide and 1900-μm long main fluidic channel with four deep recesses filled with metal microspheres connecting to planar Pt electrodes (black blocks). The microfluidic chip was equipped with two sets of inlets (inlets 1 and 2) and outlets (outlets 1 and 2). Figure 4b shows the detailed design of the main microchannel, arc-shaped 3D electrodes and the planar Pt electrodes. All microchannels are 100-μm deep including the deep recesses where the 3D electrodes are located. Each 3D electrode was designed to be 100-μm apart. This fabrication technique utilized the unique property of low melting point metal alloy to construct 3D arc-shaped electrodes protruding from the sidewall of the PDMS microchannel. Compared with most metals with melting temperature higher than 500 °C, the proposed alloy could be easily made to have good electric contact with Pt planar electrodes. If other metals were applied, the annealing process may change the property of PDMS due to the high temperature (higher than 500 °C for most metals). However, the annealing temperature for Bi metal alloy was 60 °C in our experiment, which had no influence on other materials used. To investigate the shape of 3D electrode, a fabricated

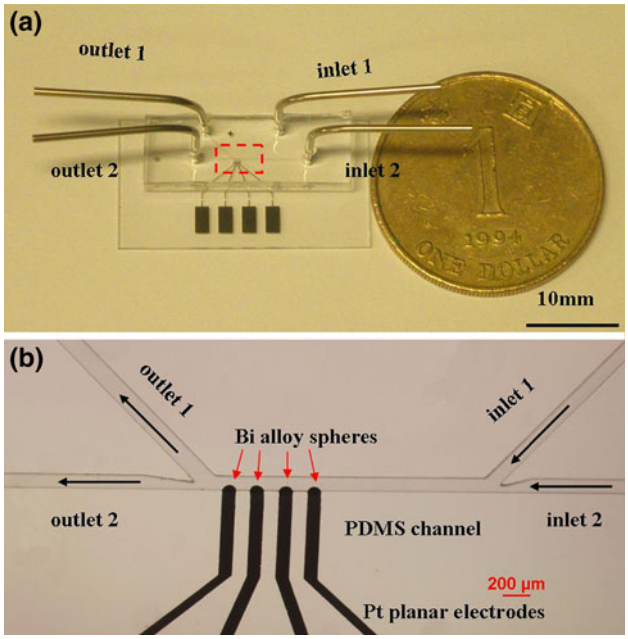

Fig. 4 **a** Microfluidic device with 3D arc-shaped electrodes at the sidewall of channel. **b** The enlarged picture of *red dashed line* circled in (**a**)

chip was cut along the channel centerline and the SEM pictures are shown in Fig. 5a–c. Figure 5b, c shows the enlarged pictures of highlighted areas indicated by red dashed lines. It is clearly seen that the original shape of the sphere is maintained and the surface is smooth enough for most applications in microfluidic chip. Particles within the channels are therefore subjected to a non-uniform electric field, which is generated by 3D electrodes. Compared to conventional planar electrodes that are either at the top or at the bottom of the microchannel, electrodes at the sidewalls provide better visualization of particle motion without the need for transparent electrodes and easier manipulation of particles in a continuous flow.

3.3 DEP responses of different type of particles

To confirm the application of fabricated microfluidic chip, manipulation of particles was conducted using DEP. Dielectrophoresis refers to the motion of polarizable biology cells and particles suspended in fluid, induced by a spatially non-uniform electric field. Particles move toward the regions of strong electric field if they are more polarized than the surrounding medium and such motion is called positive dielectrophoresis. Alternatively, if the particles are less polarizable than the medium, they move away from the regions of strong electric field, and the resultant motion is called negative dielectrophoresis (Khoshmanesh et al. 2010). The time-averaged DEP force acting on a spherical

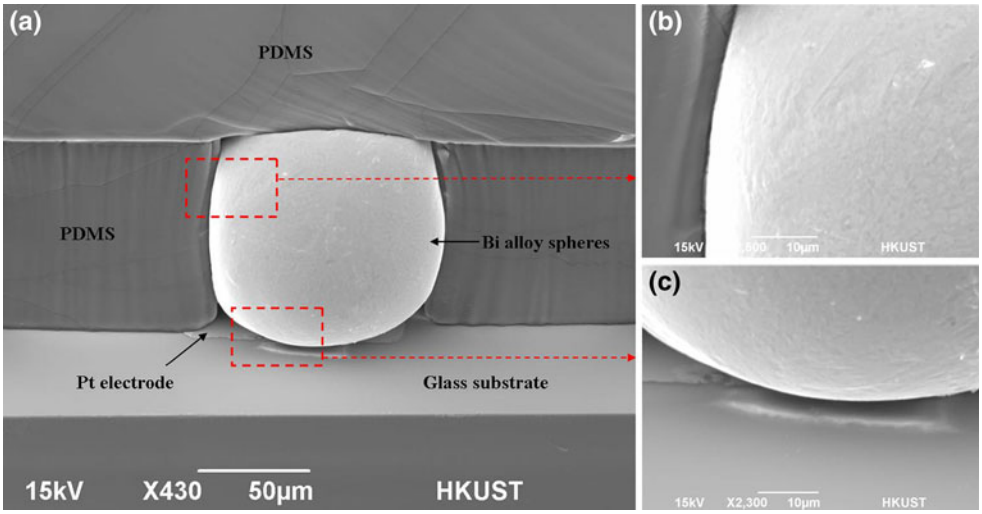

Fig. 5 **a** The SEM picture of 3D electrodes which is surrounded by PDMS and contact to planar Pt electrode, **b** and **c** are the enlarged pictures highlighted by *red dashed rectangles* in (**a**)

particle with radius a and suspended in a medium with electric permittivity of ε_m is given by (Jones 1995):

$$\left\langle \vec{F}_{DEP} \right\rangle = 2\pi\varepsilon_m a^3 \mathrm{Re}[K^*(\omega)]\nabla\left|\vec{E}_{rms}\right|^2 \quad (1)$$

where $\langle\ \rangle$ denotes the average operator with respect to time, Re[ ] is the real part of a complex number, a represents the radius of the particle, $\nabla\left|\vec{E}_{\mathrm{rms}}\right|^2$ represents the gradient of the square of the electric field and $K^*(\omega)$ is the complex Clausius–Mossotti (CM) factor, which is represented by:

$$K^*(\omega) = \frac{\varepsilon_p^* - \varepsilon_m^*}{\varepsilon_p^* + 2\varepsilon_m^*} \quad (2)$$

where $\varepsilon_{\mathrm{p}}^*, \varepsilon_{\mathrm{m}}^*$ represent the complex permittivity of particle and suspension medium and the complex permittivity is defined as $\varepsilon^* = \varepsilon - \frac{i\sigma}{\omega}$, in which $i = \sqrt{-1}$, σ is the electric conductivity and ω is the angular frequency of the applied electric field. The positive or negative DEP response of the particles is governed by the CM factor. Particles experience positive DEP when $\mathrm{Re}[K^*(\omega)]$ is a positive number; in contrast, negative DEP appears when $\mathrm{Re}[K^*(\omega)]$ is negative.

To get rid of electrolysis and adjust the DEP response for different particles and cells, AC signals with different amplitudes and frequencies were applied to the 3D arc-shaped electrodes. Electrolysis is induced by an electric current passing through an ionic substance. It is determined by the voltage applied to the electrodes, the frequency of the AC electric field and the ion concentration of the medium. In our experiment with medium conductivity of 380 μS/cm, we found that the applied voltage higher than 35 V will induce electrolysis. Increment of frequency will reduce this effect. Thus, one has to choose a suitable amplitude and frequency according to the desired DEP force and avoid potential electrolysis. All the applied AC signals would not induce noticeable electrolysis in our experiment. Figure 6 compares the trajectories of different particles without and with an electric field. Figure 6a shows the design principle of the device. As shown in Fig. 6a1, particles or cells introduced via inlet 2 were pushed toward outlet 2 by hydrodynamic force when no electric field was applied to the electrodes. However, particles or cells were deflected from the electrodes due to the negative DEP force acting on them if AC electric signal was applied to the electrodes as illustrated in Fig. 6a2. Under the influence of DEP force, particles or cells were propelled to the upper channel and collected at outlet 1. This kind of device configuration could be applied to cell/particle manipulation in a continuous flow by adjusting the applied AC signal. Figure 6b2, c2 shows the response of 10-μm PS particles and yeast cells, respectively, when they passed through an array of 3D electrodes. The applied AC signals were 15 V at 20 kHz; 25 V at 100 kHz for Fig. 6b2, c2, respectively. Our designed chip successfully manipulated the flow of PS particles and cells between inlets and outlets. The particles and cells with different trajectories are marked by red dashed circles in Fig. 6b, c. It is noticed that the amplitudes and frequencies are chosen in the region where particles exhibit strong DEP force to redirect them between two outlets. DEP responses of particles were consistent with another previous work (Lewpiriyawong et al. 2011).

3.4 Particle–particle and particle–cell separation

Based on the prediction that DEP force is proportional to the cube of particle radius according to Eq. (1), PS particle separation is shown in Fig. 7a, in which the 10-μm PS

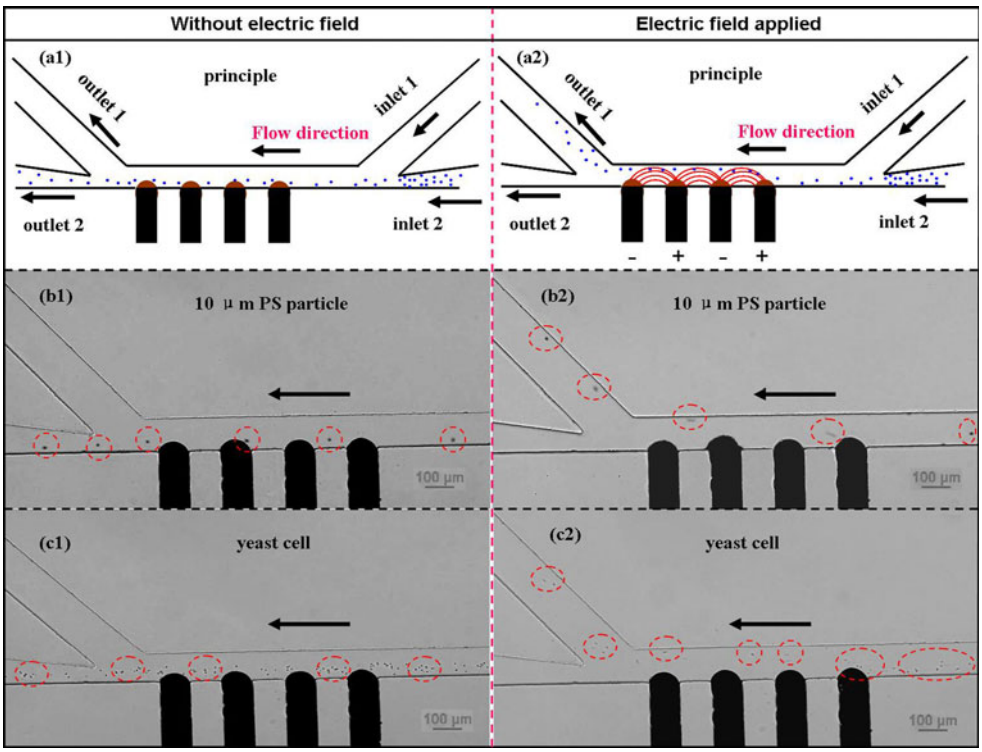

Fig. 6 Comparison of the trajectories of particles without and with electric signals applied to the 3D electrodes: **a1** and **a2** Schematic showing the working principle of the fabricated device based on DEP; **b1**, **b2**, **c1** and **c2** are the real pictures of 10-μm polystyrene particles and yeast cells in a continuous flow when they pass through the electrodes. The applied AC signals were 15 V at 20 kHz and 25 V at 100 kHz for (**b2**), (**c2**), respectively. The microparticles and cells are marked to illustrate the trajectories. Flow rate for two inlets in (**b1**), (**b2**), (**c1**) and (**c2**) are fixed at 0.1 μl/min

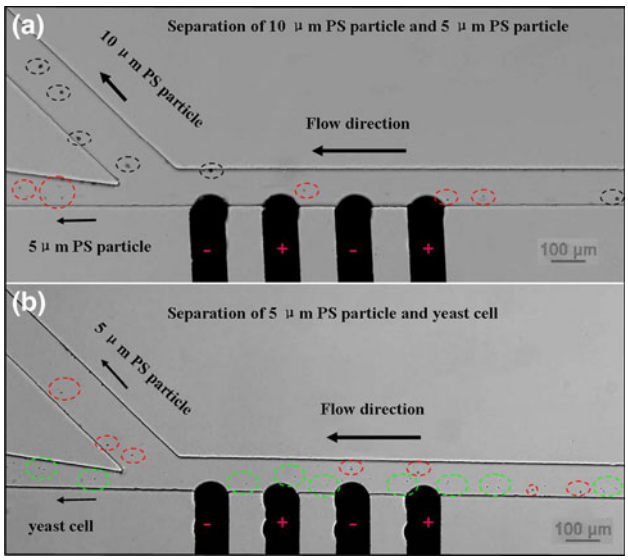

Fig. 7 **a** Separation of 10μm PS particles from a mixture of 10 and 5-μm PS particles. AC sinusoidal signal with amplitude of 15 V at 20 kHz was used. **b** The snapshot image showing the particle/cell separation process in a continuous flow with AC signal of 20 V at 200 kHz. The PS particles and cells are marked to indicate the separation process. 10-μm PS particles are marked with *black dashed circles*, 5-μm PS particles are marked with *red dashed circles* and the yeast cells are marked with *green dashed circles*

particles are marked with black dashed circles and 5-μm PS particles with red dashed circles. In the absence of an electric field, a mixture of particles of 5 and 10 μm in size was hydrodynamically focused near the channel wall where the 3D electrodes were located. When AC sinusoidal signal of 15 V at 20 kHz was applied to the two pairs of electrodes, 10-μm PS particles were deflected toward the upper channel (outlet 1), while 5-μm PS particles were directed to the lower channel (outlet 2). It is noted that the 10-μm PS particles experienced a larger negative DEP force, while the 5-μm ones experienced proportionally smaller DEP force. Therefore, the device successfully demonstrated the separation of PS particles of different sizes.

The functioning of separation based on dielectric properties was examined by sorting yeast cells and 5-μm PS particles. The 5-μm PS particles were used because they were similar in size to the yeast cells. Figure 7b shows a still image of the particle–cell separation process under an AC signal of 20 V at 200 kHz. It was observed that the 5-μm PS particles experienced a larger negative DEP force than yeast cells (Lewpiriyawong et al. 2011). The yeast cells stayed close to one side of the channel where the electrodes were located and were directed to outlet 2 on the downstream. On the other hand, 5-μm PS particles were deflected to outlet 1 on the downstream under a co-flow rate of 0.1 μl/min (the flow rate for two inlets are both 0.1μl/min). In order to clearly indicate the separation process, 5-μm PS particles and yeast cells were marked with red and green dashed circles, respectively, in Fig. 7b.

Our experimental results have shown the controllable performance of the fabricated microfluidic chip, in which particle–particle and particle–cell separations were successfully

demonstrated based on AC-DEP. The particle separation process was performed in a continuous flow manner, which allowed parallel and in situ processing of sample mixture. The separation efficiency was larger than 95 % as calculated by the statistical method at the two outlets. Also, the flow rate could be increased to obtain a higher throughput. The device was reliable after repeated working for many times. It is expected that the presented fabrication method could be applied to other designs and applications in microfluidics.

4 Conclusions

We have developed a novel and relatively simple method to fabricate a microfluidic device with 3D electrodes using metal alloy microspheres. Compared to other techniques, the presented method is unique in that 3D arc-shaped electrodes were constructed, which could provide excellent non-uniform electric field distribution in the lateral direction of the channel. It is noted that the geometry of electrodes is crucial for applications requiring non-uniform electric field such as DEP. Such arc-shaped electrodes are preferable for the manipulation of particles and cells using DEP, since they are able to generate stronger lateral DEP forces acting on the particles/cells in a continuous flow. In addition, reduction of electric field divergence is another advantage of this design since electrodes have no sharp edges. The device fabricated by presented method demonstrated its application in particle/cell manipulation under the influence of AC-DEP. The performance of the device on particle manipulation was confirmed by successfully deflecting 10-μm PS particles and yeast cells. Moreover, the function of separation was also demonstrated by separating 10-μm PS particles from 5-μm PS particles based on the size effect and separating 5-μm PS particles from yeast cells according to their difference in dielectric properties. The presented novel technique could also be used to construct 3D electrodes with different sizes and geometries on the sidewall of microchannel by applying varying-shaped metal alloy, e.g., cylinder or asymmetric shape, as long as one uses different ways to fabricate this electrode with different shapes. These proposed 3D electrodes are guaranteed by the fact that the low temperature annealing step will maintain the original shape of manually positioned electrodes as stated in the fabrication method section.

Acknowledgments This work is supported by Hong Kong RGC grant 604710 and 605411, respectively.

References

Cetin B, Kang Y, Wu Z, Li D (2009) Continuous particle separation by size via AC-dielectrophoresis using a lab-on-a-chip device with 3-D electrodes. Electrophoresis 30:766–772

Cheng I-F, Hou D, Chang H-C (2007) An integrated dielectrophoretic chip for continuous bioparticle filtering, focusing, sorting, trapping, and detecting. Biomicrofluidics 1:021503-1-021503-15

Choi J-W, Rosset S, Niklaus M, Adleman JR, Shea H, Psaltis D (2010) 3-dimensional electrode patterning within a microfluidic channel using metal ion implantation. Lab Chip 10:783–788

Chunag C-H, Chen Y-C, Hsu Y-M, Huang H-S, Hsiao F-B, Wang C-H (2009) A DEP chip with arc-shape microelectrode arrays for the separation of different-size particles. Proceedings of the 2009 4th IEEE international conference on nano/micro engineered and molecular systems 5–8 Jan 2009, Shenzhen, China, pp 854–857

Gong X, Yi X, Xiao K, Li S, Kodzius R, Qin J, Wen W (2010) Wax-bonding 3D microfluidic chips. Lab Chip 10:2622–2627

Huang C–C, Bazant MZ, Thorsen T (2010) Ultrafast high-pressure AC electro-osmotic pumps for portable biomedical microfluidics. Lab Chip 10:80–85

Iliescu C, Lin G, Samper V, Tay FE (2005) Fabrication of a dielectrophoretic chip with 3D silicon electrodes. J Micromech Microeng 15:494–500

Iliescu C, Tresset G, Xu G (2009) Dielectrophoretic field-flow method for separating particle populations in a chip with asymmetric electrodes. Biomicrofluidics 3:044104-1-044104-10

Jones TB (1995) Electromechanics of particles. Cambridge University Press, Cambridge

Khoshmanesh K, Zhang C, Nahavandi S, Tovar-Lopez FJ, Baratchi S, Mitchell A, Kalantar-zadeh K (2010) Size based separation of microparticles using a dielectrophoretic activated system. J Appl Phys 108:034904-1-034904-8

Lewpiriyawong N, Yang C (2012) AC-dielectrophoretic characterization and separation of submicron and micron particles using sidewall AgPDMS electrodes. Biomicrofluidics 6:012807

Lewpiriyawong N, Yang C, Lam YC (2010) Continuous sorting and separation of microparticles by size using AC dielectrophoresis in a PDMS microfluidic device with 3-D conducting PDMS composite electrodes. Electrophoresis 31:2622–2631

Lewpiriyawong N, Kandaswamy K, Yang C, Ivanov V, Stocker R (2011) Microfluidic characterization and continuous separation of cells and particles using conducting poly(dimethyl siloxane) electrode induced alternating current-dielectrophoresis. Anal Chem 83:9579–9585

Li M, Li S, Wu J, Wen W, Li W, Alici G (2012) A simple and cost-effective method for fabrication of integrated electronic-microfluidic devices using a laser-patterned PDMS layer. Microfluid Nanofluid 12:751–760

Lu K-Y, Wo AM, Lo Y-J, Chen K-C, Lin C-M, Yang C-R (2006) Three dimensional electrode array for cell lysis via electroporation. Biosens Bioelectron 22:568–574

Ma W, Shi T, Tang Z, Liu S, Malik R, Zhang L (2011) High-throughput dielectrophoretic manipulation of bioparticles within fluids through biocompatible three-dimensional microelectrode array. Electrophoresis 32:494–505

Mahalanabis M, Al-Muayad H, Kulinski MD, Altman D, Klapperich CM (2009) Cell lysis and DNA extraction of gram-positive and gram-negative bacteria from whole blood in a disposable microfluidic chip. Lab Chip 9:2811–2817

Niu X, Peng S, Liu L, Wen W, Sheng P (2007) Characterizing and patterning of PDMS-based conducting composites. Adv Mater 19:2682–2686

Numthuam S, Kakegawaa T, Anadab T, Khademhosseinic A, Suzukia H, Fukuda J (2011) Synergistic effects of micro/nano modifications on electrodes for microfluidic electrochemical ELISA. Sens Actuators B 156:637–644

Park BY, Madou MJ (2005) 3-D electrode designs for flow-through dielectrophoretic systems. Electrophoresis 26:3745–3757

Park J, Kim B, Choi SK, Hong S, Lee SH, Lee K (2005) An efficient cell separation system using 3D-asymmetric microelectrodes. Lab Chip 5:1264–1270

Pethig R (2010) Review article-dielectrophoresis: status of the theory, technology, and applications. Biomicrofluidics 4:022811-1-022 811-35

Senousy YM, Harnett CK (2010) Fast three dimensional AC electro-osmotic pumps with nonphotolithographic electrode patterning. Biomicrofluidics 4:036501-1-036501-7

Voldman J, Gray ML, Toner M, Schmidt MA (2002) A microfabrication-based dynamic array cytometer. Anal Chem 74:3984–3990

Wang L, Flanagan LA, Jeon NL, Monuki E, Lee AP (2007) Dielectrophoresis switching with vertical sidewall electrodes for microfluidic flow cytometry. Lab Chip 7:1114–1120

Whitesides GM (2006) The origins and the future of microfluidics. Nature 442:368–373

Wu D, Qin J, Lin B (2008) Review electrophoretic separations on microfluidic chips. J Chromatogr A 1184:542–559

Xia Y, Whitesides GM (1998) Soft lithography. Annu Rev Mater Sci 28:153–184

Yu C, Vykoukal J, Vykoukal DM, Schwartz JA, Shi L, Gascoyne PRC (2005) A three-dimensional dielectrophoretic particle focusing channel for microcytometry applications. J Microelectromech Syst 14:480–487

Yu L, Shen Z, Mo J, Dong X, Qin J, Lin B (2007) Microfluidic chip-based cell electrophoresis with multipoint laser-induced fluorescence detection system. Electrophoresis 28:4741–4747

Zeng S, Pan X, Zhang Q, Lin B, Qin J (2011) Electrical control of individual droplet breaking and droplet contents extraction. Anal Chem 83:2083–2089